



ELSEVIER

Available online at www.sciencedirect.com

 ScienceDirect

Proceedings of the Combustion Institute 31 (2007) 3319–3326

Proceedings
of the
Combustion
Institute

www.elsevier.com/locate/proci

Investigation of NO production and flame structure in plasma enhanced premixed combustion

Wooyoung Kim, Hyungrok Do, M. Godfrey Mungal^{*}, Mark A. Cappelli

Mechanical Engineering Department, Stanford University, Stanford, CA 94305-3032, USA

Abstract

A pulsed plasma source is used to stabilize lean premixed methane flames. Nitric oxide (NO) production is measured using probe sampling and chemiluminescence analysis. While the discharge is a potential source of NO, it is observed that the flame also consumes some NO. The NO production in the flame is modeled by use of a modified opposed diffusion flame simulation (OPPDIF), augmented by the initial radical pool created by the discharge. The simulations are in qualitative and quantitative agreement with the measurements, despite the simplified modeled geometry. The structure of this plasma assisted premixed flame is discussed within the framework of two interacting premixed streams, as simulated by the OPPDIF configuration. Under certain conditions, we observe a cold pre-flame associated with the plasma-excited premixed stream, the products of which (OH radicals) have an unusually high vibrational temperature and low rotational temperature in electronically excited states, when compared to the OH characteristics found in a conventional lean premixed flames. While the role of the OH radicals in this cold pre-flame stream is not fully understood, we believe it plays an important role in igniting the surrounding combustible mixture, as confirmed by the simulations.

© 2006 The Combustion Institute. Published by Elsevier Inc. All rights reserved.

Keywords: Plasma; Stabilization; Nitric oxide; Flame structure; Nonequilibrium

1. Introduction

The use of plasma discharges to enhance flame stability has received greater attention during the last decade. This renewed interest is primarily due to: (i) an increasing trend towards ultra-lean combustion to obtain low nitric oxide emissions; (ii) a growing concern to use low grade fuels to expand the fuel base; (iii) limitations associated with other stabilizing methods such as a pilot flame and recirculation/swirl, which add complexity to the overall system; and (iv) the development

of high power combustion systems such as hypersonic propulsion concepts.

It is believed that nonequilibrium plasma discharges can be an efficient source of radicals that can accelerate the reaction kinetics of the combustion processes in a relatively low translational temperature environment. In fact, promising results have been reported in the literature on the increase in flame stability using corona, dielectric barrier, and ultra short-pulse repetitive discharges (USRD) [1–9]. However, few of these studies investigate the associated impact of the plasma on nitric oxide (NO) production.

Nitric oxide production in conventional combustion systems can be categorized into four primary mechanisms: thermal, prompt, nitrous oxide and NO production due to nitrogen in the

^{*} Corresponding author. Fax: +1 650 723 1748.

E-mail address: mungal@stanford.edu (M. Godfrey Mungal).

fuel [10,11]. Among these mechanisms, the thermal NO mechanism is the most sensitive to temperature change, becoming less important at very lean conditions. However, when a plasma discharge is added to the system, the thermal mechanism becomes more difficult to unravel, since the system is removed from thermal equilibrium and vibrational and electronic temperatures can be considerably different from the translational temperature of the mixture. For example, the discharge generates electronically excited molecules of N_2 , and radicals such as OH, CN, CH and H amongst others, while the translational temperature of the system is only ~ 400 K. These excited molecules or radicals can alter the critical NO production mechanisms. Unusually high concentrations of electronically excited N_2 can disturb the following reaction:



which is an important thermal NO rate-controlling reaction, or it may lead to faster NNH production that can then produce NO by reactions with atomic oxygen:



Super-equilibrium concentrations of OH generated by a cold plasma can also accelerate NO production through the following reaction, which is often important in thermal NO mechanisms



Furthermore, CN produced in the discharge can lead to similar NO formation as that of fuel-bound-nitrogen NO formation in a conventional flame. The abundance of CH can produce additional NO through a process similar to the generation of prompt NO. Finally, NO production due

to collisions with electrons should also be considered [12]:



The above discussion implies that altered NO production in plasma stabilized combustion should also be considered in assessing the benefits of plasma stabilization, even though plasmas can extend combustion into the very lean regime.

Our current study is aimed at providing insight into the NO production in a methane/air pre-mixed flame that is stabilized by an ultra short-pulse repetitive discharge (USRD). It is shown that the resulting flame is characterized by an unusual structure which impacts the production of NO. The flame structure is characterized by optical emission spectroscopy and planar laser-induced fluorescence (PLIF) of CH radicals. NO concentrations are measured downstream of the plasma discharge using a chemiluminescence analyzer.

2. Experimental setup

Figure 1 is a schematic diagram of the experimental setup used for flame imaging (Fig. 1a) including details on the two premixed burners (Fig. 1b and c). The burner shown in Fig. 1c is a conventional lip stabilized burner of inner diameter of 45 mm. For convenience, the analysis of the NO concentration downstream of the plasma excitation, was carried out in the swirl stabilized meso-scale 6×6 array burner [13] shown in Fig. 1b, with each individual burner containing a meso-scale (2.4 mm) swirler. The

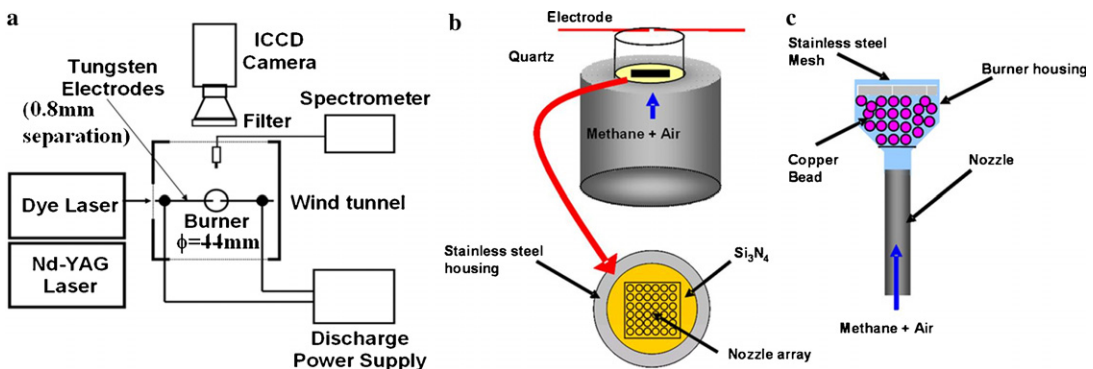


Fig. 1. Schematic of the experimental setup. (a) Setup overview. (b) Meso-scale array burner. (c) Conventional premixed nozzle.

diameter of individual burner elements for the array is 4.5 mm and the overall burner diameter is 44 mm. A detailed description of this particular meso-scale burner is given in Ref. [13]. The structure of the plasma-excited flame was similar in the two burners. The conventional burner shown in Fig. 1c was used for the PLIF studies since this facility was already conveniently in place for similar studies of plasma-stabilized diffusion flames in co-flow and crossflow conditions [1]. In both cases, the burner flow velocity is determined by measuring pressure and volume flow rate. Control of equivalence ratio is carried out by use of critical flow orifices. Measurements of NO in the array burner were made by collecting samples with an uncooled 0.8 mm diameter quartz probe and delivering these to a NO analyzer which works on the principle of the chemiluminescence reaction between NO and ozone: $\text{NO} + \text{O}_3 \rightarrow \text{NO}_2 + \text{O}_2 + h\nu$.

The USRD is generated with a 6 kV peak voltage (typically), 10 ns pulse firing at a rate of 15 kHz. Electrode pairs are constructed from 0.8 mm diameter tungsten (W) wires with blunted tips. The electrode separation is 0.8 mm. A close examination of the USRD reveals that the plasma has filamentary characteristics. The voltage and current at the electrode is recorded with a 1000:1 high voltage probe (Tektronics P6015A) and a Rogowski coil (Pearson Electronics, model 2877), respectively. Both signals are acquired simultaneously on a high-speed digital oscilloscope. The typical peak current measured at the peak voltage of 6 kV is 15 A, corresponding to a peak power of 90 kW. As mentioned above, in some cases, we recorded a survey of the plasma emission with a spectrometer that has a spectral resolution of 0.17 nm (Ocean Optics S2000). For obtaining higher resolution spectra over a limited spectral range, we imaged the emission onto a 0.75 m focal length SPEX 750M spectrometer that is equipped with a 2000 × 800 pixel CCD camera at the exit plane.

For CH planar laser-induced fluorescence (PLIF) imaging, the 60 mJ/pulse output from a Nd:YAG (Spectra Physics Pro 290) pumped dye laser (Sirah Precision Scan) tuned to 390.23 nm is shaped into a sheet and directed into the flame. This wavelength excites the $Q_1(7)$ transition of the $B_2\Sigma^- \leftarrow X^2\Pi(0,0)$ band [14]. The resulting fluorescence is detected using an intensified CCD camera (Princeton Instruments PI-MAX) which is triggered at 3 Hz with a 75 ns gate width. An Exalite 389/398 dye mixture is used to generate the excitation wavelength and a combination of thick (3 mm) KV-418 and BG-3 Schott glass filters were used to block the broad-band flame radiation and the elastic scattering from particles near 390 nm, while the CH fluorescence (430 nm) can pass through them [14].

3. Results and discussion

3.1. Measurement of nitric oxide production

With the electrode pair placed downstream of the meso-scale burner, single point measurements were first carried out of the NO concentration above a plasma discharge in pure ambient air. As expected, the discharge generated a significant level of NO, typically 80–100 ppm at a height of 10 mm above the discharge and 10 mm towards the cathode side from the center of the discharge. This amount of NO production is large when compared to that generated by combustion in this meso-scale burner (~ 10 ppm at an equivalence ratio, $\phi = 0.72$) [15]. However, it is noteworthy that the NO concentration resulting from the discharge is highly localized and hence non-uniform, and its spatially burner-averaged level is estimated to be as low as 5 ppm. It is this spatially-averaged level that is more appropriately compared to the NO concentration seen uniformly over the two-dimensional burner under normal combustion conditions. The uncertainty of the NO measurements conducted in this study is estimated to be approximately $\pm 10\%$. This error is primarily caused by the pressure fluctuation during the sampling process ($\pm 10\%$) in addition to the inaccuracy of the NO analyzer ($\pm 1\%$), the bias error resulting from undesirable quenching of the sample gas with other species (CO_2 and O_2 , +2%) and uncertainty due to probe reactions (+0.1%) [16].

Figure 2 shows the spatial distribution of NO concentration at a height of 10 mm above the electrode, along the electrode direction for three different equivalence ratios, $\phi = 0, 0.33$ and 0.49 . It is apparent that the concentration of NO is strongly biased towards the cathode side. We attribute this to the possibility that most of the radicals generated by the discharge are produced in the vicinity of the cathode by collisions between

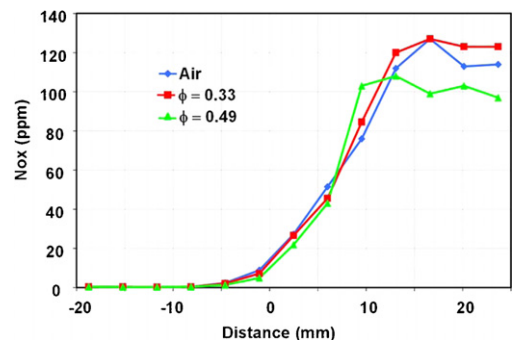


Fig. 2. NO concentration distribution along electrode direction at 10 mm above the electrode. NO production is strongly biased to the cathode side (positive values).

accelerated electrons and neutral molecules. For a discharge in pure air, the measured NO concentration is below the sensitivity of the detector beyond a position of 5 mm from the center of the discharge on the anode side. Within approximately 10 mm, the concentration rises steeply, and levels off to a value of 120 ppm on the cathode side. When methane is added to the air (non-zero ϕ), the trend is similar but the height of the plateau is slightly higher. We attribute this slight increase in the NO level to a modest increase in the discharge power. Increased power dissipation will lead to an increase in reactive species responsible for NO formation, such as excited N_2 , O, OH, etc. The peak voltage and current measurements support the possible discharge power increase due to the slight addition of methane, since in comparison with the pure air case, the $\phi = 0.33$ case shows 5% higher peak current with the identical peak voltage. However, when the equivalence ratio is further increased (e.g., to $\phi = 0.49$), a visible flame appears (ignition) coincident with a drop in the NO concentration by about 20% near the plateau region. Since the spatial location of the plateau corresponds also to the location of the first visible flame, a reduction (albeit slight) of NO above the cathode side suggests that the flame partially consumes the NO produced by the discharge. It seems that in a plasma-stabilized premixed flame, the plasma may be the main source of NO whereas the flame partially consumes it, similar to a reburn process.

In Fig. 3, the normalized NO concentration is shown as a function of equivalence ratio at two different spatial locations, one 10 mm above the center of the electrodes, and the other 10 mm above the visible flame center whose radial position is ~ 10 mm towards the cathode side from

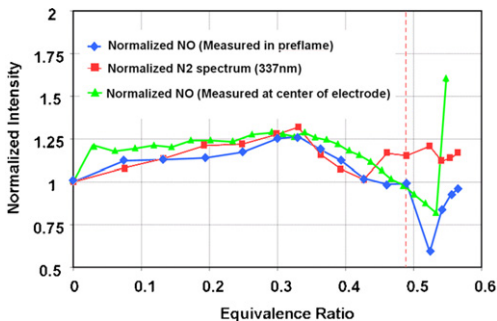


Fig. 3. Normalized NO concentration as a function of equivalence ratio. Sampling is done at two different locations. NO consumption of the pre-flame is clearly seen. In addition, before the flame ignition, the intensity of the N_2 C-B (0, 0) emission is well correlated to NO production. The red dotted line represents the start of the visible flame. (For interpretation of the references to color in this figure legend, the reader is referred to the web version of this paper.)

the electrode center. The NO concentration is seen to slowly increase with increasing equivalence ratio up to a value of $\phi = 0.3$. This gradual increase is believed to be due to improved power coupling to the gas, as mentioned earlier. However, a further increase in equivalence ratio beyond 0.3 reverses the trend. This drop in NO concentration is also attributed to the change in the power dissipation, as the increase in methane mole fraction gives rise to reduced plasma conductivity. The overall behavior suggests that there is an optimum equivalence ratio for Ohmic dissipation, established by a balance between the introduction of more easily ionizable species at low equivalence ratio, and a reduction in electron mobility at too high an equivalence ratio. This is supported by the trend seen in the emission intensity of the 2nd positive system of $N_2(0,0)$, shown as red squares in the figure. The intensity of the emission should be a reflection of the power coupling to the plasma, and agrees well with the trend seen in NO concentration before flame ignition, represented by the vertical dashed line in Fig. 3. At equivalence ratios just beyond flame ignition, there is a notable decrease of NO level consistent with the earlier result seen in Fig. 2 especially at the flame center (blue diamonds). This phenomenon is also apparent in the data taken from the electrode center region (green triangles). It is noteworthy that there is no corresponding drop in the emission intensity, suggesting that the change in NO signal is not due to a change in discharge power coupling.

Just beyond an equivalence ratio of $\phi = 0.52$, the trend suddenly reverses again, and there is a sudden increase in NO concentration. We attribute this increase to the introduction of another NO formation mechanism related perhaps to the thermal NO production often seen in low equivalence ratio flames, but affected here by the presence of the discharge.

To better understand this rise in NO concentration, we have carried out a preliminary modeling effort of the plasma-affected kinetics using a modified version of the opposed flow strained diffusion flame simulation, OPPDIF [17] that incorporates the GRI MECH 3.0 [18] chemical kinetics mechanism. We use OPPDIF here with opposed premixed flows under lean conditions, with one flow seeded with a concentration of radicals generated by the pulsed plasma discharge and the other consisting of the unseeded lean mixture. The radical containing flow represents a portion of the premixed flow in the burner that passes through the discharge region. The boundary temperature of this radical containing flow is taken to be 400 K (based on spectroscopic studies of the discharge), is assumed to be at ambient pressure (1 atm) and is assumed to have an entering velocity of 1 m/s (streamwise velocity of the mixture). For the non-plasma activated side, the tempera-

ture is taken to be 300 K and the velocity and pressure are equal to that of the radical containing flow.

To simulate the role that the initial plasma formation may have on flame ignition and NO production, we calculate initial radical yields as described by Penetrante [19], based on the electron collision induced fragmentation of parent fuel and air molecules. This requires a solution (using the commercial solver BOLSIG [20]) of the Boltzmann equation for the electron energy distribution function (EEDF), knowing the discharge reduced electric field ($E/n \sim 250$ Td). The EEDF subsequently allows us to calculate the dissociation reaction rates and the electron mobility, from which we can determine the fraction of the total dissipated energy that is needed to produce radicals from the parent gases. Reactions considered are the electron impact dissociation of molecular nitrogen, oxygen and methane (producing CH_3 and H). The determined yield of N, O, CH_3 and H, together with the known average discharge power leads to the initial radical production rates. The concentrations of these radicals are then determined from the known pressure, flow temperature, flow rate, and effective plasma area through which a portion of the flow passes. This latter parameter is adjusted to reproduce the peak NO concentration measured. For the results presented here, an area of $\sim 20 \text{ mm}^2$ is found to predict NO levels comparable to those measured. A second check on the reasonableness of this area is the resulting ability of the simulation to predict the lean flammability limit.

The computed spatial variation in the NO and OH concentration is shown in Fig. 4. In this simulation, the separation between the opposed flow boundaries is 1 cm and $\phi = 0.525$. The separation between the flows is chosen to approximately reproduce the flow strain rate expected in typical

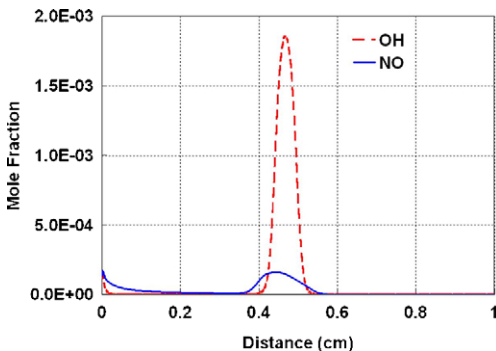


Fig. 4. Calculated NO (solid blue) and OH (dotted red) concentration of the plasma/flame system. The flame reaction zone is located near 0.47 cm. (For interpretation of the references to color in this figure legend, the reader is referred to the web version of this paper.)

premixed flame experiments [21]. The radical containing flow is located at the left boundary. The simulation predicts the flame location (based on the peak in the OH concentration) to be at a distance of approximately 0.47 cm. The NO concentration is seen to rise to ~ 170 ppm. An examination of the kinetics indicates that within the first 0.1 mm (very near the plasma stream boundary) reactions which influence the NO production are $\text{N} + \text{O}_2 \rightarrow \text{NO} + \text{O}$ and $\text{N} + \text{OH} \rightarrow \text{NO} + \text{H}$. However, beyond 0.1 mm the initial NO concentration decreases, as a result of the $\text{NO} + \text{N} \rightarrow \text{O} + \text{N}_2$ reaction.

3.2. Flame structure

Figure 5 illustrates a picture of a premixed flame stabilized by a USRD operated at 50 kHz and 6 kV. Two main observations can be made. First, the discharge aided flame shows a highly asymmetric flow stream tendency. Even though it is not provided here, particle image velocimetry (PIV) confirms that our discharge forms a highly skewed reacting flow. As mentioned earlier, we believe this is also due to the influence of the applied electric field on ion radicals produced by the flame and discharge. Second, there is an unusual white emission, which we refer to as the ‘pre-flame,’ at the center region of the flame surrounded by the usual blue colored flame referred to here as the ‘main flame.’

To understand the origin of this white emission, we examined the spectra of this pre-flame, an example of which is shown in Fig. 6. The black curve represents spectral emission originating from the discharge while the green curve is the spectral emission from a location 3 mm above the discharge, within the pre-flame. The emission originating from the discharge is dominated by molecular nitrogen, whereas that from the pre-

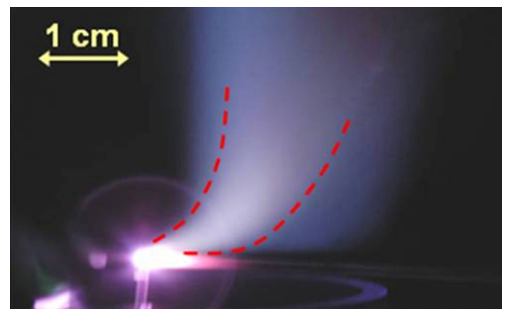


Fig. 5. Marginally stabilized methane jet in a premixed flame. White colored emission is detected in the pre-flame. A visible boundary between the pre-flame and main flame is represented by red dotted lines. Flow speed ~ 1 m/s. (For interpretation of the references to color in this figure legend, the reader is referred to the web version of this paper.)

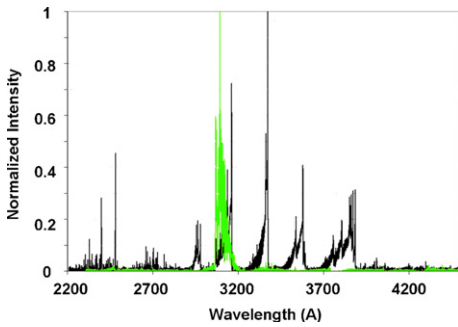


Fig. 6. Emission spectra of the discharge (black) and of the pre-flame located 3 mm above the discharge (green). (For interpretation of the references to color in this figure legend, the reader is referred to the web version of this paper.)

flame is dominated by the OH radical. The results of the simulations described in the previous section reasonably predict this occurrence of the dominant species. They indicate that the OH concentration immediately increases to ~ 160 ppm, while the other species such as H, CH₃, N and O drop in value by over 99.9% of their initial values very near the discharge. As expected, we find that the rate of production of the OH is controlled by reactions with hydrogen and oxygen atoms ($\text{H} + \text{HO}_2 \rightarrow \text{OH} + \text{OH}$ and $\text{H} + \text{HO}_2 \rightarrow 2\text{OH}$).

Figure 7 compares two of the measured OH spectra. The green curve is the OH emission spectra obtained from the main flame while the black curve is obtained from the pre-flame. The detection location of the main flame is 5 mm downstream from the electrode and 2 cm towards the cathode electrode while that of pre-flame is 3 mm downstream and 5 mm towards the cathode. Compared to that of the main flame, the pre-flame spectrum has a relatively lower peak

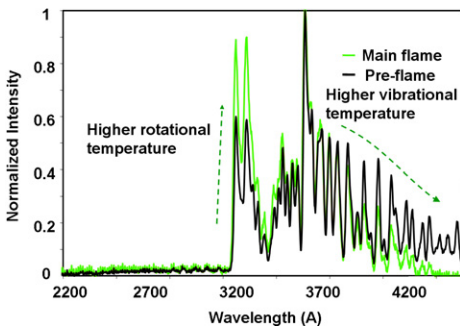


Fig. 7. Detailed OH emission spectra from the main flame (green) and from the pre-flame (black). The OH in pre-flame has lower rotational temperature and higher vibrational temperature. (For interpretation of the references to color in this figure legend, the reader is referred to the web version of this paper.)

near 307 nm, implying a low rotational temperature, and is relatively broader, implying a higher vibrational temperature. The existence of two apparently different OH populations, in the center and the outer regions, suggests the presence of a layered structure to this flame. This is supported in part by the simulations in Fig. 4. While the OH concentration is high just downstream of the discharge and subsequently decays as it recombines, another peak appears at the flame boundary, once flame ignition occurs. The differences in the temperatures reflected in the spectra are attributed to the possibility that the emission from the main flame is expected to be rotationally (translationally) hot, whereas the emission from the near-plasma region is expected to be vibrationally hot, consistent with our experimental observation. Finally, it is noteworthy that we observed the characteristics of the pre-flame to be very long lived. It appears that the high vibrational/low rotational temperature persists to great distances, in some cases to as much as 9 cm above the burner. This implies that a fluid element which passes through the discharge can have ~ 110 ms residence time without losing its initial high vibrational and low rotational temperature characteristic. However, this observation is not reflected by the results of the simulation, which shows that the distance between the first (near the discharge) and the second (near the main flame) OH peaks in Fig. 4 is 0.47 cm. The calculated residence time of the fluid element which travels this region is ~ 6 ms which is much shorter than the observation. We believe that this discrepancy can be resolved by carrying out further refinement of the simulations which includes reaction kinetics between OH radicals and any lingering high energy electrons near the discharge.

To further understand the nature of the pre-flame and the associated OH, we collected and averaged the two-dimensional image of OH ($A-X$) emission as shown in Fig. 8a. In this figure, the flow direction is from bottom to top and the electrodes are located just below the circle. From this image the distinction of the pre-flame and outer main flame is apparent. Perhaps the most interesting region is highlighted by the circle. It appears that the main flame (distinguished by the outer emission) seems to start from the middle of the pre-flame and then propagates both upstream and downstream of this pre-flame (dotted lines). We believe this is an important feature, to be studied further, as it may suggest that the flame ignition may be due to the pre-flame OH, rather than resulting directly from the discharge.

Finally, a representative CH PLIF image of a lifted jet in crossflow flamebase is shown in Fig. 8b. The jet emits from a nozzle located at the left bottom corner of the figure with a jet speed of 14 m/s while the crossflow travels from the bottom to the top with a speed of 3.5 m/s.

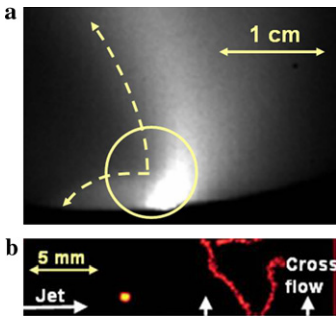


Fig. 8. (a) Intensified image of averaged OH emission. The ignition of the main flame is observed to start inside the circle shown by the dotted lines. (b) Instantaneous CH PLIF image at flamebase of a lifted jet flame. There exists ~ 1 cm gap between CH produced by discharge (bright spot) and CH produced by flame (dimmer red). The initial jet velocity and the crossflow speed are 14 m/s and 3.5 m/s, respectively. (For interpretation of the references to color in this figure legend, the reader is referred to the web version of this paper.)

Even though the flame configuration is a partially premixed lifted flamebase rather than a fully premixed case, the image is consistent with the above conjecture that the flame front does not originate at the discharge, but rather, at some distance from the discharge, anchored perhaps by the presence of the pre-flame. In this image, the discharge region is the bright spot, and the flamebase location is the randomly shaped CH line to the right of the discharge. An examination of numerous similar images confirms that the two CH regions are usually separated, presumably by the region (rich in OH) described as the “pre-flame”. Further investigations will be aimed at understanding the role of this pre-flame on the stabilization process, and its relationship to the plasma discharge.

4. Conclusions

Nitric oxide concentration was measured in an ultra short-pulse repetitive discharge (USRD) stabilized premixed methane/air flame. While the plasma discharge could be considered as a source of NO production, a pre-flame was observed to form at low equivalence ratio, and is believed to partially consume NO. In the absence of ignition of either this pre-flame, or the main flame, the production of NO correlated well with the concentration of excited molecular nitrogen, and hence the power deposition by the plasma. Following the ignition of the main flame at higher equivalence ratio, the NO was seen to rise abruptly.

Preliminary simulations of the NO production were carried out using the initial radical pool created by the discharge as an input to the commer-

cially available OPPDIF flame code. Reasonable agreement between predictions and experiments are obtained.

The flame studied here exhibited a dual layer structure. A dominant species in the “pre-flame,” OH, was identified by emission spectroscopy. The emission from OH in this pre-flame persists for many centimeters downstream of the discharge, and is vibrationally hot and rotationally cold. Finally, a combination of CH PLIF, emission measurements and the simulation of OH concentration was used to highlight the possible role that the OH radical may play in linking the discharge kernel to the main flame through this pre-flame. The simulation results showed two independent OH peaks, as observed experimentally, however, it was unable to predict the long persistence characteristic of the OH through the pre-flame.

Acknowledgments

This work is sponsored by the AFOSR/MURI Program—Experimental/Computational Studies of Combined-Cycle Propulsion: Physics and Transient Phenomena in Inlets and Scramjet Combustors, Julian Tishkoff, Technical Monitor. We would like to thank S. Lee and C.F. Edwards for providing access to the meso-scale array burner and NO chemiluminescence analyzer, and C.-H. Lim for cross section data.

References

- [1] W. Kim, H. Do, M.G. Mungal, M.A. Cappelli, 44th AIAA Aerospace Sciences Meeting and Exhibit, AIAA-2006-0560, 2006.
- [2] W. Kim, H. Do, M.G. Mungal, M.A. Cappelli, *Parametric Study of Flame Stabilization and NO Production in a Plasma Assisted Methane/Air Premixed Flame*, WSS/CI Fall Meeting 05F-78, Stanford, CA, 2005.
- [3] M.S. Cha, S.M. Lee, K.T. Kim, S.H. Chung, *Combust. Flame* 141 (2005) 438–447.
- [4] T. Ombrello, X. Qin, Y. Ju, S. Gangoli, A. Gutsol, A. Fridman, 44th AIAA Aerospace Sciences Meeting and Exhibit, AIAA-2006-1214, 2006.
- [5] E.I. Mintousov, A.A. Nikipelov, S.M. Starikovskaia, A. Yu. Starikovskii, 44th AIAA Aerospace Sciences Meeting and Exhibit, AIAA-2006-0614, 2006.
- [6] S.M. Starikovskaia, N.B. Anikin, I.N. Kosareve, N.A. Popov, A.Yu. Starikovskii, 44th AIAA Aerospace Sciences Meeting and Exhibit, AIAA-2006-0616, 2006.
- [7] D. Galley, G. Pilla, D. Lacoste, S. Ducruix, F. Lacas, D. Veynante, C.O. Laux, 43rd AIAA Aerospace Sciences Meeting and Exhibit, AIAA-2005-1193, 2005.
- [8] S. Pancheshnyi, D.A. Lacoste, A. Bourdon, C.O. Laux, *Propane–Air Mixture Ignition by a Sequence of Nanosecond Pulses*, European Conference for Aerospace Sciences, 2005.

- [9] G. Lou, A. Bao, M. Nishihara, S. Keshav, Y.G. Utkin, I.V. Adamovich, 44th AIAA Aerospace Sciences Meeting and Exhibit, AIAA-2006-1215, 2006.
- [10] C.T. Bowman, in: C. Vouelle (Ed.), *Pollutants from Combustion*, Kluwer Publishers, Netherlands, 2000, p. 123.
- [11] J. Warnatz, U. Maas, R.W. Dibble, *Combustion*, Springer, Berlin, 2001, p. 237–256.
- [12] W.G. Vincenti, C.H. Kruger, *Introduction to Physical Gas Dynamics*, Krieger Publishing Company, 1986, p. 165.
- [13] S. Lee, C.F. Edwards, C.T. Bowman, ASME Int. M.E. Congress and RD&D Expo, Paper IMECE 2004-61050, 2004.
- [14] C.D. Carter, J.M. Donbar, J.F. Driscoll, *Appl. Phys.* 66 (1998) 129–132.
- [15] S. Lee, M. Svrcek, C.F. Edwards, C.T. Bowman, *J. Propul. Power* 22 (2006) 417–424.
- [16] C.C. Schmidt, Report No. TSD-133, Stanford University, 2000.
- [17] A.E. Lutz, R.J. Kee, J.F. Grcar, F.M. Rupley, Report No. SAND96-8243, Sandia National Laboratory, 1997.
- [18] Available at <http://www.me.berkeley.edu/gri-mech/version30>.
- [19] B.M. Penetrante, M.C. Hsiao, B.T. Merritt, G.E. Vogtlin, P.H. Wallman, M. Neiger, O. Wolf, T. Hammer, S. Broer, *Appl. Phys. Lett.* 68 (1996) 3719–3721.
- [20] Available at <http://www.siglo-kinema.com/bolsig.htm>.
- [21] M.G. Mungal, L.M. Lourenco, A. Krothapalli, *Combust. Sci. Tech.* 106 (1995) 239–265.